Co monolayers and adatoms on Pd(100), Pd(111), and Pd(110): Anisotropy of magnetic properties

O. Šipr,[1,*] S. Bornemann,[2] H. Ebert,[2] S. Mankovsky,[2] J. Vackář,[1] and J. Minár[2]
[1]*Institute of Physics of the ASCR v. v. i., Cukrovarnická 10, CZ-162 53 Prague, Czech Republic*
[2]*Universität München, Department Chemie, Butenandtstr. 5-13, D-81377 München, Germany*
(Received 21 March 2013; revised manuscript received 4 June 2013; published 13 August 2013)

We investigate to what extent the magnetic properties of deposited nanostructures can be influenced by selecting as a support different surfaces of the same substrate material. Fully relativistic *ab initio* calculations were performed for Co monolayers and adatoms on Pd(100), Pd(111), and Pd(110) surfaces. Changing the crystallographic orientation of the surface has a moderate effect on the spin magnetic moment, a larger effect on the orbital magnetic moment, but sometimes a dramatic effect on the magnetocrystalline anisotropy energy and on the magnetic dipole term T_α. The dependence of T_α on the magnetization direction α can lead to a strong apparent anisotropy of the spin magnetic moment as deduced from the x-ray magnetic circular dichroism sum rules. For systems in which the spin-orbit coupling is not very strong, the T_α term can be understood as arising from the differences between components of the spin magnetic moment associated with different magnetic quantum numbers m.

DOI: 10.1103/PhysRevB.88.064411 PACS number(s): 75.70.Ak, 75.30.Gw, 78.70.Dm, 73.22.Dj

I. INTRODUCTION

The magnetic properties of surface-deposited nanostructures have been in the ongoing focus of many experimental and theoretical investigations as they often exhibit interesting and sometimes unexpected phenomena. One of the main features in this context is that the local magnetic moments and their mutual interaction as well as the magnetocrystalline anisotropy energy (MAE) are in general different and often much larger in nanostructures than in corresponding bulk systems. Various aspects of the magnetism of many different nanostructures were studied in the past to identify the key factors which could then be used to tune the properties of such systems in a desired way. It has been known for a long time that such important key factors are, for example, reduction in atomic coordination number as well as symmetry breaking, which play a crucial role for magnetic properties of surfaces and deposited nanosystems. Their effect is reflected, for instance, in the trend of surfaces and clusters to have larger atomic magnetic moments and stronger magnetocrystalline anisotropy when compared to bulk systems.[1–3] Naturally, however, these factors alone are far from sufficient to fully determine the magnetism of nanostructures as also other factors such as the chemical composition play a significant role. An Fe monolayer, for instance, has a larger spin magnetic moment when deposited on Au(111) than when deposited on Pt(111), whereas for a Co monolayer it is the other way around.[3] The situation is even more diverse for the MAE where different substrates may lead to different properties of systems of otherwise identical geometries. For example, Co_2 and Ni_2 dimers on Pt(111) have out-of-plane magnetic easy axis but the same dimers on Au(111) have an in-plane magnetic easy axis.[3]

Thus, a deeper theoretical understanding of the magnetism of nanostructures is needed to support the interpretation of corresponding experiments. Here, one of the most widely used experimental techniques in this field is the x-ray magnetic circular dichroism (XMCD) spectroscopy in combination with its theoretically derived sum rules.[4–6] The strength of these sum rules is that they give access to spin magnetic moments $\mu_{\rm spin}$ and orbital magnetic moments $\mu_{\rm orb}$ separately, and this in a chemically specific way.[7,8] However, the XMCD spin sum rule does not provide $\mu_{\rm spin}$ alone but only its combination $\mu_{\rm spin} + 7T_\alpha$, where T_α is the magnetic dipole term (for the magnetization $\boldsymbol{M}$ parallel to the α axis, $\alpha = x, y, z$).[7] For bulk systems, T_α can be usually neglected, but for surfaces and clusters the T_α term can have significant influence, as it has been demonstrated experimentally[9,10] and theoretically.[11–13] The anisotropy of the magnetic dipole term was predicted on general grounds[14] and some estimates concerning the magnitude of this anisotropy in noncubic bulk systems were given based on atomiclike model Hamiltonians[14] or on *ab initio* calculations.[15]

Magnetic nanostructures may be prepared by combining and arranging different magnetic elements on different substrates. In this respect, one can also address surfaces of different crystallographic orientations and it is important to know how the magnetic properties can be controlled by selecting for the substrate crystallographically different surfaces of the same material and whether one can expect different effects for complete monolayers and for adatoms. Connected with this is the question about the effects on the T_α term and how this influences the values of magnetic moments deduced from the XMCD sum rules. For planning and interpreting related experiments, it would thus be very useful not only to know the T_α values from *ab initio* calculations, but also to have a simple and intuitive interpretation of the T_α term.

In order to learn more about this, we undertook a systematic study of Co monolayers and adatoms on Pd(100), Pd(111), and Pd(110) surfaces. Investigating such a comprehensive set of systems via the same computational scheme allows us to make direct comparisons which would otherwise be hindered by technicalities if individual results for different systems were taken over from other available studies which rely on different computational schemes. Fully relativistic *ab initio* calculations were performed to obtain $\mu_{\rm spin}$, $\mu_{\rm orb}$, and T_α for different magnetization directions. The MAE was determined for all these systems as well. The accuracy of an approximative expression for the T_α term was examined to

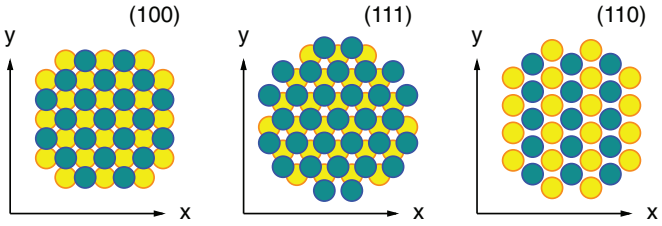

FIG. 1. (Color online) Structure diagrams for a Co monolayer on Pd(100), Pd(111) and Pd(110). The blue and yellow circles represent the Co and Pd atoms, respectively. The orientation of the x and y coordinates used throughout this paper is also shown.

verify that it captures the essential physics and that it can be used as a basis for a more intuitive understanding of the T_α term. It is shown in the following that monolayers and adatoms on different crystallographic surfaces may have indeed quite different magnetic properties, especially as concerns the MAE. Moreover, it is also demonstrated how the dependence of the T_α term on the magnetization direction leads to a surprisingly strong apparent anisotropy of μ_{spin} as deduced from the XMCD sum rules.

II. METHODS

A. Investigated systems

We investigated Co monolayers on Pd(100), Pd(111), and Pd(110) and also Co adatoms on the same surfaces. The corresponding structure diagrams are shown in Fig. 1 (for adatoms, obviously only one Co atom is kept). Two hollow adatom positions are possible for the (111) surface, differing by the position of the adatom with respect to the subsurface layer; we consider the fcc position in this work (unless specified otherwise).

The Pd substrate has fcc structure with lattice constant $a = 3.89$ Å. To determine the distances between the Co atoms and the substrate, we relied in most cases on the "constant volume approximation": the vertical Co-Pd interplanar distance $z_{\text{Co-Pd}}$ is taken as an average between the interlayer distance in bulk Pd and the interlayer distance in a hypothetical pseudomorphically grown fcc Co film compressed vertically in such a way that the atomic volume of Co is the same as in bulk Co.[16] In addition, we took also into account relevant experimental data and results of *ab initio* geometry relaxations when available. For example, the constant volume approximation yields $z_{\text{Co-Pd}} = 1.70$ Å for a Co monolayer on Pd(100) while we took $z_{\text{Co-Pd}} = 1.65$ Å instead, following the surface x-ray diffraction experiment of Meyerheim *et al.*[17] For the other two surfaces, we used the constant-volume-approximation distances, namely, $z_{\text{Co-Pd}} = 1.96$ Å for Co on Pd (111) and $z_{\text{Co-Pd}} = 1.20$ Å for Co on Pd(110). In the case of the (111) surface, we can compare our distance with an EXAFS-derived experimental distance $z_{\text{Co-Pd}} = 2.02$ Å (Ref. 18) and with an *ab initio* equilibrium distance $z_{\text{Co-Pd}} = 1.91$ Å (Ref. 19). It follows from this comparison that the constant volume approximation leads to reasonable distances.

Systems with interplanar distances as given above will be called systems with "optimized geometries." Apart from that, we investigate for comparison also systems where the Co atoms are located in ideal positions of the underlying Pd lattice. For this, we use the designation "bulklike geometry." The interplanar distances are summarized in Table I.

TABLE I. Vertical distances $z_{\text{Co-Pd}}$ in Å between the plane containing Co atoms and plane containing Pd atoms for systems investigated in this study.

Surface	Optimized geometry	Bulklike geometry
(100)	1.65	1.95
(111)	1.96	2.25
(110)	1.20	1.38

For adatoms we use the same $z_{\text{Co-Pd}}$ distances as for monolayers. This is a simplification because the constant volume approximation will work worse for adatoms than for monolayers. For example, the *ab initio* $z_{\text{Co-Pd}}$ distance for a Co adatom on Pd(111) is 1.66 Å (Ref. 20) in contrast to our optimized geometry value of 1.96 Å. However, by using identical $z_{\text{Co-Pd}}$ distances for monolayers and adatoms, the net effect due to the change in Co coordination can be studied. It will be shown that the effect of varying the distances is in fact smaller than the effect of monolayer-to-adatom transition.

B. Computational scheme

The calculations were performed within the *ab initio* spin density functional framework, relying on the local spin density approximation (LSDA) with the Vosko, Wilk, and Nusair parametrization for the exchange and correlation potential.[21] The electronic structure is described, including all relativistic effects, by the Dirac equation, which is solved using the spin-polarized relativistic multiple scattering or Korringa-Kohn-Rostoker (SPR-KKR) Green's function formalism[22] as implemented in the SPR-TB-KKR code.[23] The potentials were treated within the atomic sphere approximation (ASA) and for the multipole expansion of the Green's function, an angular momentum cutoff $\ell_{\max} = 3$ was used.

The electronic structure of Co monolayers on Pd surfaces was calculated by means of the tight-binding or screened KKR technique.[24] The substrate was modeled by slabs of 13–14 layers (i.e., a thickness of 17–27 Å, depending on the surface orientation), the vacuum was represented by 4–5 layers of empty sites. The adatoms were treated as embedded impurities: first, the electronic structure of the host system (clean surface) was calculated and then a Dyson equation for an embedded impurity cluster was solved.[25] The impurity cluster contains 135 sites if not specified otherwise; this includes a Co atom, 50–60 Pd atoms, and the rest are empty sites.

It should be stressed that the embedded clusters define the region where the electronic structure and potential of the host is allowed to relax due to the presence of the adatom and *not* the size of the considered system. In this respect, the Green's function approach differs from the often used supercell approach: there is an unperturbed host beyond the relaxation zone in the former approach, while in the latter approach, the supercell is terminated either by vacuum or by another (interfering) relaxation zone pertaining to an adjacent adatom. The sizes of the embedded clusters and the sizes of

the supercells thus have a different meaning and can not be directly compared.

The MAE is calculated by means of the torque $T_{\hat{u}}^{(\hat{n})}$ which describes the variation of the energy if the magnetization direction $\hat{n}$ is infinitesimally rotated around an axis $\hat{u}$. To present the relation between the MAE and the torque for systems with no symmetry, we start with the expression for the total energy expanded up to the second order in directions cosines:[26]

$$\begin{aligned} E(\theta,\phi) = {} & E_0 + K_{2,1}\cos 2\theta + K_{2,2}(1-\cos 2\theta)\cos 2\phi \\ & + K_{2,3}(1-\cos 2\theta)\sin 2\phi + K_{2,4}\sin 2\theta\cos\phi \\ & + K_{2,5}\sin 2\theta\sin\phi. \end{aligned} \quad (1)$$

The difference in energy between in-plane and out-of-plane magnetization is then

$$\begin{aligned} & E(90^\circ,\phi) - E(0^\circ,\phi) \\ & = -2K_{2,1} + 2K_{2,2}\cos 2\phi + 2K_{2,3}\sin 2\phi \\ & = \left.\frac{\partial E(\theta,\phi)}{\partial\theta}\right|_{\theta=45^\circ}. \end{aligned} \quad (2)$$

So, the MAE we are interested in can be obtained just by evaluating the torque for $\theta = 45^\circ$.[27] The torque itself was calculated by relying on the magnetic force theorem.[28]

Apart from the magnetocrystalline anisotropy induced by the spin-orbit coupling (SOC), the magnetic easy axis is also determined by the so-called shape anisotropy caused by magnetic dipole-dipole interactions. The shape anisotropy energy is usually evaluated classically by a lattice summation over the magnetostatic energy contributions of individual magnetic moments, even though it can be in principle obtained *ab initio* via a Breit Hamiltonian.[29] In this paper, we always deal only with the magnetocrystalline contribution to the magnetic anisotropy unless stated otherwise.

III. RESULTS

A. Magnetic moments and magnetocrystalline anisotropy

To assess the effect of selecting different crystallographic surfaces and of going from a monolayer to an adatom, we calculated magnetic moments and the MAE for all these systems. The results are summarized in Table II. For each system, the data are shown first for the optimized geometry and then for the bulklike geometry (numbers in the parentheses). The x, y, and z superscripts in the column header labels indicate the direction of the magnetization $\boldsymbol{M}$.

The spin magnetic moment μ_{spin} is shown only for $\boldsymbol{M} \parallel z$ because it is practically independent on the magnetization direction: by varying it, μ_{spin} can be changed by no more than 0.2%. On the other hand, for μ_{orb} the differences can be quite large. The second in-plane magnetization direction $\boldsymbol{M} \parallel y$ was investigated only for the (110) surface because there is only very small "intraplanar anisotropy" for the (100) and (111) surfaces (this issue is addressed in more detail in Sec. III C). For bulk hcp Co we get $\mu_{\text{spin}} = 1.61\ \mu_B$ and $\mu_{\text{orb}} = 0.08\ \mu_B$.

Changing the surface orientation has a moderate effect on μ_{spin}: the differences in μ_{spin} when going from one surface to another are at most 9%. However, the situation is quite different for μ_{orb} where the differences are 20%–50%. The sensitivity in μ_{orb} finds its counterpart in the sensitivity of the MAE. For example, the magnetic easy axis for a Co monolayer is in plane for the (100) and (110) surfaces but out of plane for the (111) surface. For the adatom, the easy axis is in plane for the (110) surface, but out of plane for the (100) and (111) surfaces. So, in this respect the choice of the crystallographic surface can have a dramatic influence.

Another finding emerging from Table II is that as concerns μ_{spin}, the difference between monolayers and adatoms is only quantitative in most cases. A surprisingly small difference in this respect is found for the (110) surface. As the same Co-Pd

TABLE II. Magnetic properties of Co monolayers and adatoms on Pd(100), Pd(111), and Pd(110). The first column specifies whether the values are for a monolayer or for an adatom, and the second column contains spin magnetic moment for the Co atom for $\boldsymbol{M} \parallel z$ (in units of μ_B). The third, fourth, and fifth columns contain orbital magnetic moments for the Co atom for $\boldsymbol{M} \parallel z$, $\boldsymbol{M} \parallel x$, and $\boldsymbol{M} \parallel y$, respectively. The last three columns contain the MAE between indicated magnetization directions (in meV per Co atom). Numbers without parentheses stand for systems with optimized Co-Pd distances, and numbers in parentheses stand for systems with a bulklike geometry (see Sec. II A).

	$\mu_{\text{spin}}^{(z)}$	$\mu_{\text{orb}}^{(z)}$	$\mu_{\text{orb}}^{(x)}$	$\mu_{\text{orb}}^{(y)}$	$E^{(x)} - E^{(z)}$	$E^{(y)} - E^{(z)}$	$E^{(x)} - E^{(y)}$
			Co on Pd(100)				
Monolayer	2.09	0.132	0.203		−0.73		
	(2.07)	(0.190)	(0.241)		(−0.69)		
Adatom	2.29	0.299	0.279		0.26		
	(2.32)	(0.610)	(0.473)		(2.69)		
			Co on Pd(111)				
Monolayer	2.02	0.135	0.136		0.36		
	(1.99)	(0.154)	(0.176)		(0.21)		
Adatom	2.35	0.605	0.355		5.50		
	(2.34)	(0.780)	(0.575)		(6.38)		
			Co on Pd(110)				
Monolayer	2.15	0.192	0.183	0.210	−0.15	−0.43	0.28
	(2.18)	(0.215)	(0.220)	(0.289)	(−0.48)	(−0.97)	(0.49)
Adatom	2.20	0.270	0.347	0.201	−1.51	1.10	−2.61
	(2.25)	(0.349)	(0.472)	(0.255)	(−1.88)	(2.01)	(−3.89)

distances have been used for monolayers and adatoms, one observes here the net effect of the change in Co coordination. For $\mu_{\rm orb}$, the difference between monolayers and adatoms is obviously much larger than for $\mu_{\rm spin}$. For the MAE, this difference can again be substantial: The magnetic easy axis for a Co monolayer on Pd(100) is in plane, while for a Co adatom on the same surface it is out of plane. Similarly, the magnetic easy axis for a monolayer on Pd(110) is parallel to the y axis, while for an adatom it is parallel to the x axis.

Changing the distance between Co atoms and the surface clearly affects the magnetic properties (cf. the values with and without parentheses in Table II). However, it is noteworthy that the effect of geometry relaxation is smaller than the effect of the transition from the monolayer to the adatom.

We calculated also the magnetic shape anisotropy for the monolayers (classically, via a lattice summation, taking into account also moments on Pd atoms). As expected, this contribution favors always an in-plane orientation of the magnetization. For Co monolayers on Pd(100) and Pd(111), we get $E^{(x)}_{\text{dip-dip}} - E^{(z)}_{\text{dip-dip}} = -0.1$ meV. For Co monolayers on Pd(110), there is a small difference regarding the x and y directions: we get $E^{(x)}_{\text{dip-dip}} - E^{(z)}_{\text{dip-dip}} = -0.07$ meV and $E^{(y)}_{\text{dip-dip}} - E^{(z)}_{\text{dip-dip}} = -0.09$ meV. By comparing these values with the values shown in Table II, we see that the shape anisotropy energy is smaller in magnitude than the magnetocrystalline anisotropy energy and thus the shape anisotropy does not change the orientation of the magnetic easy axis as determined by the magnetocrystalline anisotropy.

The large amount of data gathered here for quite a complete set of systems allow a comprehensive look at the relation between the MAE and the anisotropy of $\mu_{\rm orb}$. In this respect, Bruno's formula[30]

$$E^{(\alpha)} - E^{(\beta)} = -\frac{\xi}{4}\left[\mu^{(\alpha)}_{\rm orb} - \mu^{(\beta)}_{\rm orb}\right] \qquad (3)$$

connecting the differences of total energies to the differences of orbital magnetic moments for two orientations of the magnetization α and β proved to be very useful[31] despite its limitations,[32] which become more severe in the case of multicomponent systems with large SOC parameter ξ for the nonmagnetic component.[33,34] Moreover, this proportionality between MAE and $\mu_{\rm orb}$ was questioned also on general grounds, using a model Hamiltonian.[35] To assess the situation for $3d$-$4d$ alloys, we compare the differences $\Delta\mu_{\rm orb}$ and ΔE, using all the appropriate values given in Table II. The outcome is shown in Fig. 2, together with a straight line representing Eq. (3). We take $\xi = 85$ meV for the SOC parameter [which appears to be a rather universal value for Co as our calculations yield ξ of 85.4, 84.5, 84.9, and 85.1 meV for bulk hcp Co and for a Co monolayer on Pd(100), Pd(111), and Pd(110), respectively].

It follows from Fig. 2 that Bruno's formula (3) works quite well for adatoms (albeit with some "noise") but not so well for monolayers, where relying solely on Eq. (3) might even lead to a wrong sign of the MAE (in case of small absolute values). This may be connected with the fact that if the MAE is not large, small absolute deviations from the rule given in Eq. (3) can lead to large relative errors. The deficiencies of the Bruno formula are not removed if we use instead

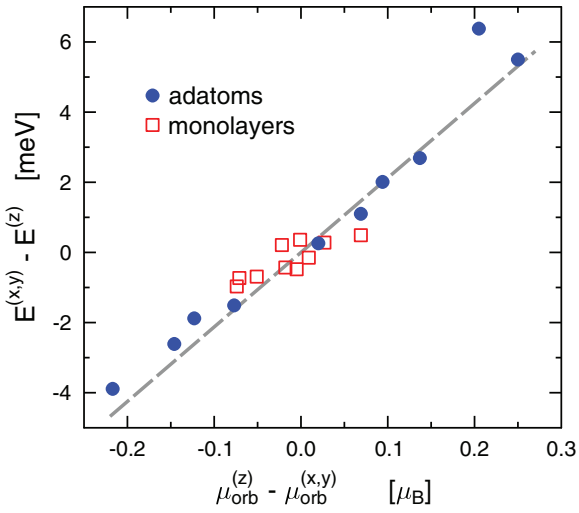

FIG. 2. (Color online) Dependence of the MAE for Co monolayers and adatoms on the difference of orbital magnetic moments for respective magnetization directions. The dashed line represents Bruno's formula in Eq. (3).

a more general formula due to van der Laan[36] (where the assumption that the majority spin band is completely filled has been relaxed); the values of the MAE obtained via the van der Laan formula change with respect to values obtained from Eq. (3) by 10%–20%, sometimes improving but sometimes worsening the agreement with the *ab initio* values of Table II.

We would like to point out two issues which are important regarding both $\mu_{\rm orb}$ and the magnetocrystalline anisotropy. First, there are mutual effects between SOC strength and hybridization of electronic states of the Co atoms with the states of the surrounding Pd atoms, as this determines the $\mu_{\rm orb}$ values of the adsorbed atoms. The second issue is the anisotropy of the electronic structure at the surface which is responsible for the anisotropy of $\mu_{\rm orb}$ as well as for the anisotropy of the total energy at different directions of magnetization in the system. Concerning different crystallographic orientations, one should expect different hybridizations for different surfaces simply because of the differences in the geometries: while the nearest Co-Pd distances are more or less the same for all three crystallographic orientations (they vary within 5% for the optimal geometry and are identical for the bulklike geometry), the coordination numbers differ. For Co on Pd(111), each Co atom has only three Pd atoms as its neighbors, so the Co-Pd hybridization is relatively weak, for Co on Pd(100) the hybridization will be stronger because there are four Pd atoms around a Co atom, and the strongest hybridization can be expected for Co on Pd(110) where each Co atom has five Pd atoms in its neighborhood (the fifth Pd atom is hidden below the Co atom in the rightmost drawing in Fig. 1).

The effect of different hybridization schemes can be seen when inspecting the density of states (DOS). We present the DOS for the Co atoms and also for the Pd atoms in the uppermost layer (nearest to the Co atoms) in Fig. 3. We display only the results for $\boldsymbol{M} \parallel z$, the corresponding curves for $\boldsymbol{M} \parallel x$ or $\boldsymbol{M} \parallel y$ would be hardly distinguishable from them at this scale (even though there are differences on a scale of about 0.1 eV). Here, a special attention should be paid to the

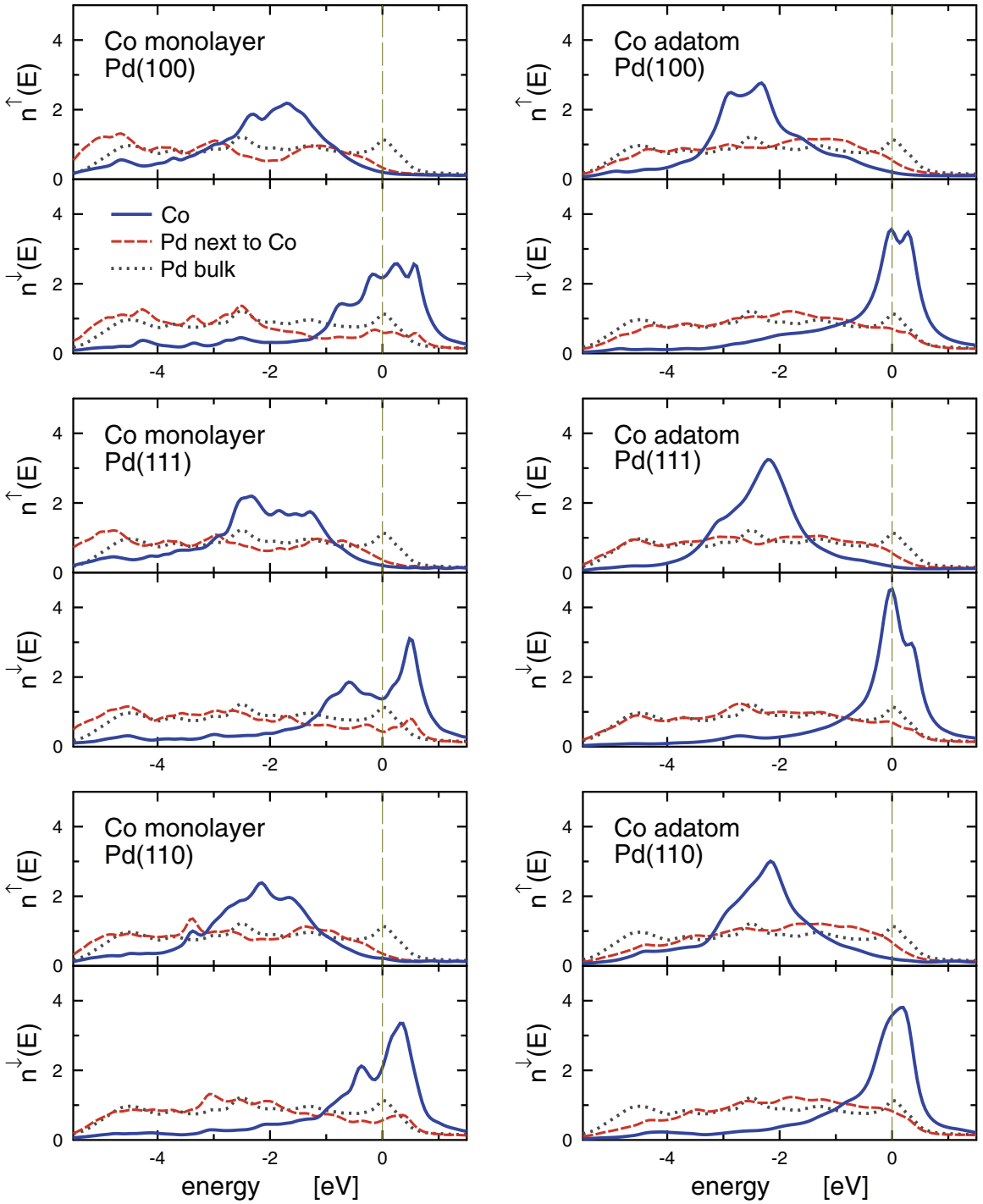

FIG. 3. (Color online) Spin-polarized DOS for Co monolayers and adatoms on Pd surfaces (in states per eV). Full lines represent DOS related to Co atoms, dashed lines represent DOS related to Pd atoms which are nearest neighbors to Co atoms, dotted lines represent DOS for bulk Pd.

minority spin states because we found that the anisotropy of μ_{orb} comes by more than 90% from the minority spin states and the same trend can be expected regarding the MAE because of the validity of the Bruno formula for our systems. One can see that there are indeed big differences in the minority spin DOS around the Fermi energy E_F for different orientations of the Pd substrate. Sometimes there is a peak in the minority DOS at E_F, sometimes a valley, sometimes a slope. The differences in the DOS suggest that from the electronic structure point of view, one is actually dealing each time with quite a different system, so it is not surprising that the differences in the MAE are large.

To get a more complete picture, we explore also how the calculated MAE depends on the position of the top of the valence band E_{band}, i.e., on the band filling. The results are shown in Fig. 4. One can see that the dependence of the MAE

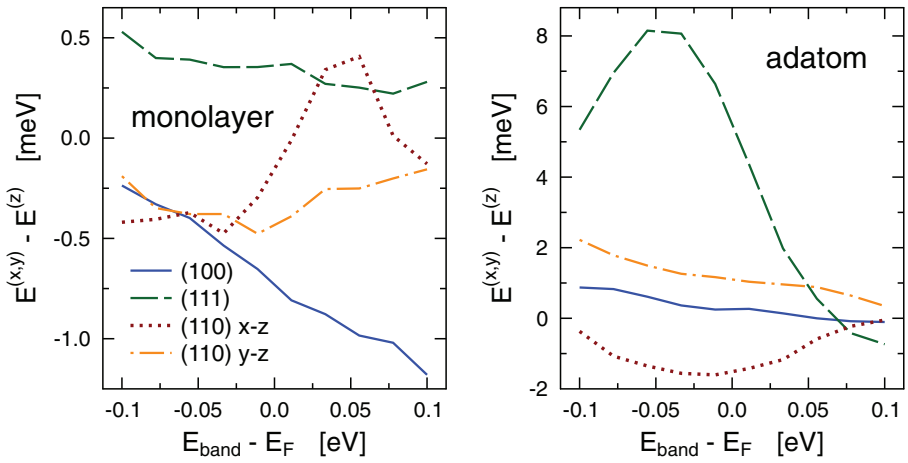

FIG. 4. (Color online) Dependence of the MAE on the position of the top of the valence band. For systems on Pd(110), the anisotropy energies $E^{(x)} - E^{(z)}$ and $E^{(y)} - E^{(z)}$ are investigated separately. The left panel is for monolayers, the right panel is for adatoms. The meaning of the lines is the same for both panels (see the legend).

on E_{band} differs for different Pd surface orientations. This is again an indication for different character of the investigated systems in this respect. It is worth noticing that for the system with by far the largest MAE, namely, Co adatom on Pd(111), the dependence of the MAE on E_{band} is very steep around the true Fermi level and that the corresponding minority spin DOS has a sharp peak at E_F.

B. Induced magnetic moments

Palladium is not magnetic as an element but it is quite polarizable.[37,38] Spin magnetic moments induced in the Pd substrate by Co monolayers and adatoms are shown in Table III for all three surface orientations. In the case of Co monolayers, the induced moments are shown for the first three atomic layers of Pd below the Co layer [denoted as Pd(1), Pd(2), and Pd(3) in Table III]. Note that the interlayer distances are 1.95, 2.25, and 1.38 Å for the (100), (111), and (110) surfaces, respectively (Table I). The relatively large μ_{spin} for the Pd(2) and Pd(3) sites in the case of the (110) surface reflects the relatively small interlayer distance for this crystallographic orientation.

TABLE III. Spin magnetic moments for Pd atoms which are first-, second-, and third-nearest neighbors of Co atoms, in units of μ_B. As in Table II, the numbers without parentheses stand for systems with optimized geometry and the numbers in parentheses stand for systems with bulklike geometry.

	Pd(1)	Pd(2)	Pd(3)
	Co on Pd(100)		
Monolayer	0.29	0.17	0.11
	(0.25)	(0.16)	(0.10)
Adatom	0.18	0.06	0.04
	(0.15)	(0.06)	(0.04)
	Co on Pd(111)		
Monolayer	0.32	0.16	0.03
	(0.25)	(0.15)	(0.06)
Adatom	0.16	0.02	0.04
	(0.12)	(0.02)	(0.03)
	Co on Pd(110)		
Monolayer	0.29	0.22	0.17
	(0.29)	(0.24)	(0.19)
Adatom	0.15	0.04	0.04
	(0.15)	(0.05)	(0.04)

In the case of adatoms, the description is formally more complicated because Pd atoms belonging to the same coordination shell around the Co atom are not all equivalent: some of them belong to the surface layer, some to the subsurface layer, and so on. In order not be overwhelmed by too much data, we display here only moments averaged over all atoms of a given coordination shell. Symbols Pd(1), Pd(2), and Pd(3) in Table III stand now for the first, second, and third shells of Pd atoms around the Co adatom. Moreover, we also calculated the orbital magnetic moments for the Pd atoms in all systems and we found that μ_{orb} amounts to about 8%–17% of the corresponding μ_{spin}.

In this section, we deal only with magnetic moments on those Pd atoms which are close to the Co atoms. The issue of more distant Pd atoms and of the total charge contained in the polarization cloud is dealt with in the Appendix. Here, we would only like to stress that it follows from the analysis outlined in the Appendix that our model system is clearly adequate to yield reliable values of induced magnetic moments for the Pd(1), Pd(2), and Pd(3) sites.

C. Azimuthal dependence of the MAE

In general, the MAE defined as the difference between total energies for in-plane and out-of-plane orientation of the magnetization will depend on the azimuthal angle ϕ. This dependence is often ignored but it may sometimes be significant for low-symmetry surfaces. In our case, the intraplanar MAE $E^{(x)} - E^{(y)}$ is quite comparable to $E^{(x)} - E^{(z)}$ or $E^{(y)} - E^{(z)}$ for the (110) surface, not only for the monolayer but also for the adatom (see Table II). To get a more complete picture, we inspect the azimuthal dependence of $E^{(\parallel)}(\phi) - E^{(z)}$, where $E^{(\parallel)}(\phi)$ is the total energy if $\boldsymbol{M}$ is in the surface plane ($\theta = 90^\circ$) with the azimuthal angle ϕ. Our results for a Co adatom on all three Pd surfaces are shown in Fig. 5. The data reported here were obtained for the optimized geometry, but the trends would be similar for any $z_{\text{Co-Pd}}$ distance.

One can see from Fig. 5 that the $E^{(\parallel)}(\phi) - E^{(z)}$ curves follow the symmetry of the appropriate surface, as expected. The amplitude of these curves is the most interesting

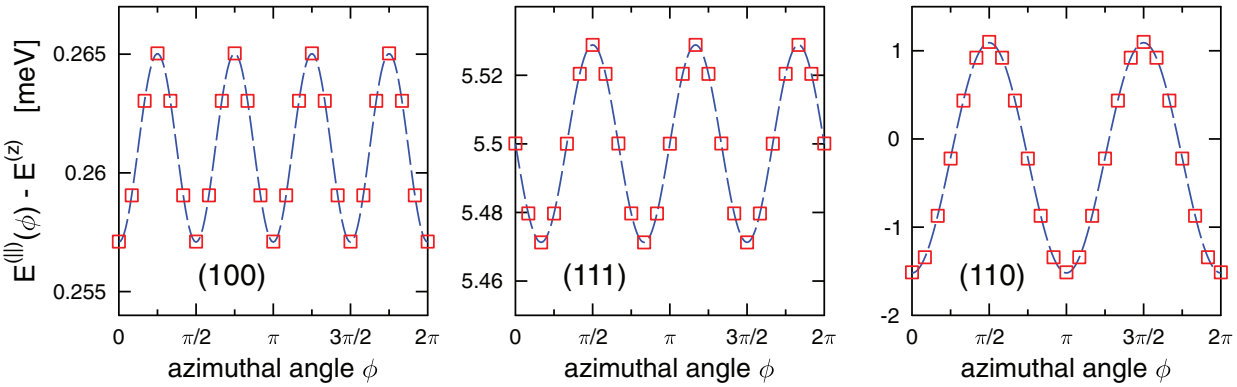

FIG. 5. (Color online) Difference between total energies for in-plane and out-of-plane magnetization for a Co adatom on Pd (100), (111), and (110) surfaces (optimized geometry). Points are results of the calculation, dashed lines are sinusoidal fits. The orientation of the x and y axes is as in Fig. 1.

information here. For high-symmetry surfaces, it is almost negligible: 0.008 meV or 3% of the average value for Co on Pd(100) and 0.06 meV or 1% of the average value for Co on Pd(111). For the (110) surface, however, the amplitude is 2.6 meV and to speak about a common uniaxial MAE does not make sense in this case, as illustrated by the fact that the magnetic easy axis is in plane for $\phi = 0^\circ$ and out of plane for $\phi = 90^\circ$.

D. Relation between magnetic dipole term and m-decomposed spin magnetic moment

The spin magnetic moment sum rule for the $L_{2,3}$ edge XMCD spectra can be written for a sample magnetized along the α direction as[7]

$$\frac{3}{I}\int \left(\Delta\mu_{L_3} - 2\Delta\mu_{L_2}\right)dE = \frac{\mu_{\text{spin}} + 7T_\alpha}{n_h}, \tag{4}$$

where $\Delta\mu_{L_{2,3}}$ are the differences $\Delta\mu = \mu^{(+)} - \mu^{(-)}$ between absorption coefficients for the left and right circularly polarized light propagating along the α direction, I is the integrated isotropic absorption spectrum, μ_{spin} is the local spin magnetic moment (only its d component enters here), n_h is the number of holes in the d band, and T_α is the expectation value of the intra-atomic dipole operator for the valence d electrons. It is often called the magnetic dipole term in the literature dealing with the XMCD. It can be also related to the magnetic dipole contribution to the magnetic hyperfine field.[39] The T_α term can be written as[40,41]

$$\begin{aligned} T_\alpha &= -\frac{\mu_B}{\hbar}\langle \hat{T}_\alpha \rangle \\ &= -\frac{\mu_B}{\hbar}\left\langle \sum_\beta Q_{\alpha\beta} S_\beta \right\rangle, \end{aligned} \tag{5}$$

where

$$Q_{\alpha\beta} = \delta_{\alpha\beta} - 3r_\alpha^0 r_\beta^0 \tag{6}$$

is the quadrupole moment operator and S_α is the spin operator. If z is the quantization axis, the eigenvalues of S_z are $\pm(1/2)\hbar$.

It follows from Eq. (5) that T_α is a measure for the quadrupole moment of the spin density. An approximate expression in terms of more intuitive quantities can be obtained if the SOC is neglected. Then, it can be shown that[14,41]

$$T_\alpha = \frac{1}{2}(-\mu_B)\sum_{mm'}[N^{\uparrow}_{mm'} - N^{\downarrow}_{mm'}]\langle Y_{2m}|\hat{Q}_{\alpha\alpha}|Y_{2m'}\rangle, \tag{7}$$

where $N^{(s)}_{mm'}$ is a spin-dependent number of states matrix defined as

$$N^{(s)}_{mm'} = \int_{-\infty}^{E_F} dE \int_{BZ} d\boldsymbol{k} \int r^2 dr\, a^{(s)*}_{E\boldsymbol{k}\ell m}(r)\, a^{(s)}_{E\boldsymbol{k}\ell m'}(r).$$

The coefficients $a^{(s)}_{E\boldsymbol{k}\ell m}(r)$ determine the expansion of the wave function in the angular momentum basis

$$\psi_{E\boldsymbol{k}}(\boldsymbol{r}) = \sum_{\ell m}\sum_{s} a^{(s)}_{E\boldsymbol{k}\ell m}(r)\, Y_{\ell m}(\hat{\boldsymbol{r}})\, \chi^{(s)}, \tag{8}$$

where a simplified two-component formulation instead of the full Dirac approach was used. We restrict ourselves to the $\ell = 2$ component only (therefore we omit the ℓ subscript from the $N^{(s)}_{mm'}$ notation).

The diagonal components of the $\langle Y_{2m}|\hat{Q}_{\alpha\alpha}|Y_{2m'}\rangle$ matrix were published in Refs. 14 and 40. Most of the nondiagonal components are zero. We summarize all the nonzero components (including the diagonal ones) in Table IV. Equation (7) makes it possible to associate the somewhat abstract T_α term with the spin magnetic moment resolved into components according to the magnetic quantum number m:

$$\mu^{(m)}_{\text{spin}} = (-\mu_B)(N^{\uparrow}_{mm} - N^{\downarrow}_{mm}).$$

TABLE IV. Nonzero components of the quadrupole operator in the basis of real spherical harmonics.

	Q_{xx}	Q_{yy}	Q_{zz}
$\langle Y_{xy}\|\hat{Q}_{\alpha\alpha}\|Y_{xy}\rangle$	$-\frac{2}{7}$	$-\frac{2}{7}$	$\frac{4}{7}$
$\langle Y_{yz}\|\hat{Q}_{\alpha\alpha}\|Y_{yz}\rangle$	$\frac{4}{7}$	$-\frac{2}{7}$	$-\frac{2}{7}$
$\langle Y_{3z^2-r^2}\|\hat{Q}_{\alpha\alpha}\|Y_{3z^2-r^2}\rangle$	$\frac{2}{7}$	$\frac{2}{7}$	$-\frac{4}{7}$
$\langle Y_{xz}\|\hat{Q}_{\alpha\alpha}\|Y_{xz}\rangle$	$-\frac{2}{7}$	$\frac{4}{7}$	$-\frac{2}{7}$
$\langle Y_{x^2-y^2}\|\hat{Q}_{\alpha\alpha}\|Y_{x^2-y^2}\rangle$	$-\frac{2}{7}$	$-\frac{2}{7}$	$\frac{4}{7}$
$\langle Y_{x^2-y^2}\|\hat{Q}_{\alpha\alpha}\|Y_{3z^2-r^2}\rangle$	$\frac{2\sqrt{3}}{7}$	$-\frac{2\sqrt{3}}{7}$	0

Namely, if we retain in the sum (7) only the terms which are diagonal in m, we get

$$T_\alpha = \sum_m \frac{1}{2} \langle Y_{2m}|\hat{Q}_{\alpha\alpha}|Y_{2m}\rangle \, \mu_{\rm spin}^{(m)}. \quad (9)$$

In the absence of SOC, Eq. (9) thus presents an exact expression for T_z and an approximate expression for T_x and T_y (due to the existence of the nondiagonal terms $\langle Y_{x^2-y^2}|\hat{Q}_{xx}|Y_{3z^2-r^2}\rangle$ and $\langle Y_{x^2-y^2}|\hat{Q}_{yy}|Y_{3z^2-r^2}\rangle$, see Table IV). As argued by Stöhr,[14,41] for high-symmetry systems the nondiagonal terms drop out of the sum in Eq. (7) altogether. Moreover, if the xz and yz orbitals are degenerate so that $\mu_{\rm spin}^{(xz)} = \mu_{\rm spin}^{(yz)}$, it can be shown [e.g., by a direct substitution from Table IV to Eq. (9)] that $T_z = -2T_x = -2T_y$ (cf. Refs. 39, 42, and 43).

The scheme outlined above gives a concrete meaning to the common statement that the magnetic dipole term T_α is related to the anisotropy of the spin density distribution. In particular, if all the m components of $\mu_{\rm spin}$ are the same, T_α will be zero [as it follows trivially from Eq. (9) and Table IV]. It is also evident from Eq. (9) and Table IV that the T_α term will generally depend on the magnetization direction α.

To get a more quantitative feeling of how the various contributions add together to generate T_α, we present in Table V the m-decomposed magnetic moment $\mu_{\rm spin}^{(m)}$ and individual terms of the sum in Eq. (9) for Co monolayers on Pd surfaces. One can see that the T_α term is formed by a competition between those m components which contain the α coordinate and those which do not (they contribute with an opposite sign, as it follows also from Table IV). One could also say that, intuitively, the magnetic dipole term T_α reflects the difference between the spin magnetic moment as seen from the α direction and as seen from the direction perpendicular to α.

TABLE V. Spin magnetic moment decomposed according to the magnetic quantum number m together with the corresponding $T_\alpha^{(m)} = \frac{1}{2}\mu_{\rm spin}^{(m)}\langle Y_{2m}|\hat{Q}_{\alpha\alpha}|Y_{2m}\rangle$ terms of the decomposition (9) for Co monolayers on Pd (optimized geometry). The sums of these components are shown in the last row for each system and they correspond to the total $\mu_{\rm spin}$, T_z, T_x, and T_y of the d electrons [evaluated using the approximative expression (9) in the case of T_α].

Component	$\mu_{\rm spin}^{(m)}$	$T_z^{(m)}$	$T_x^{(m)}$	$T_y^{(m)}$
		Co on Pd(100)		
xy	0.319	0.092	−0.046	−0.046
yz	0.465	−0.066	0.133	−0.066
$3z^2-r^2$	0.365	−0.104	0.052	0.052
xz	0.465	−0.066	−0.066	0.133
x^2-y^2	0.449	0.128	−0.064	−0.064
Sum	2.062	−0.018	0.009	0.009
		Co on Pd(111)		
xy	0.339	0.097	−0.048	−0.048
yz	0.428	−0.061	0.122	−0.061
$3z^2-r^2$	0.490	−0.140	0.070	0.070
xz	0.428	−0.061	−0.061	0.122
x^2-y^2	0.339	0.097	−0.048	−0.048
Sum	2.023	−0.069	0.034	0.034
		Co on Pd(110)		
xy	0.397	0.113	−0.057	−0.057
yz	0.346	−0.049	0.099	−0.049
$3z^2-r^2$	0.515	−0.147	0.074	0.074
xz	0.527	−0.075	−0.075	0.151
x^2-y^2	0.343	0.098	−0.049	−0.049
Sum	2.128	−0.060	−0.009	0.069

Equation (9) gives an insight into T_α provided that the underlying approximations, the neglect of the SOC and of the nondiagonal terms in Table IV, are not too crude. To check whether this really is the case, we compare the values of T_α calculated via the exact relation in Eq. (5) and via the approximative Eq. (9). Special attention is paid to the differences between the T_α terms for different orientations of $\boldsymbol{M}$ because the $7(T_\alpha - T_\beta)$ quantities determine the apparent anisotropy of $\mu_{\rm spin}$, i.e., its dependence on the direction of $\boldsymbol{M}$ as deduced from the XMCD sum rule in Eq. (4). The outcome for both monolayers and adatoms is summarized in Table VI. Let us recall that for bulk hcp Co, the magnetic dipole term is very small (we get $T_z = -0.002\ \mu_B$). Note that all values presented in Tables V and VI were obtained from fully relativistic calculations, including the SOC.

One can see from our results that the approximative expression for T_α works quite well for the Co-Pd systems: quantitative deviations sometimes occur but the main trend is well maintained. One can expect that for systems with a strong SOC, the deviations between Eqs. (5) and (9) will be larger.

The last two columns of Table VI contain the values of $7(T_x - T_z)$ and, for the case of the (110) surface, also of $7(T_y - T_z)$. These values are comparable to $\mu_{\rm spin}$, which means that even though $\mu_{\rm spin}$ practically does not depend on the magnetization direction at all, its combination $\mu_{\rm spin} + 7T_\alpha$ probed by the XMCD sum rule may strongly depend on the magnetization direction. Perhaps, we should note in this context that the number of holes n_h does not depend on the magnetization direction (we found relative variations to be less than 0.1%), so it can not hinder the use of the sum rule (4) in this respect. Likewise, choosing different Pd surface orientations changes n_h by less than 5%.

Once we have demonstrated that Eq. (9) presents a good approximation for T_α, we could speculate whether it is possible to promote the simple picture further. An inspiration can be sought in the dependence of local spin magnetic moments on the coordination numbers: lower coordination number generally means higher total ("isotropic") magnetic moment for the atom in question.[1,2,44] Within this philosophy, one could think of relating the m-resolved spin magnetic moments to "directional coordination numbers," with directions specified by appropriate spherical harmonics. Using a simple linear *ansatz*, one could then find a decomposition of the total $\mu_{\rm spin}$ into its m-dependent components and use Eq. (9) to estimate T_α. Because of the crucial role of the (directional) coordination numbers in this scheme, applying this procedure makes sense only for monolayers, not for adatoms where there are no neighbors of the same atomic type.

To test the hypothesis, we define directional m-dependent coordination numbers c_m as overlap integrals of the electron densities projected on appropriate spherical harmonics,

$$c_m = \sum_j \int d\boldsymbol{r}\, g(|\boldsymbol{r} - \boldsymbol{R}_j|)\, |Y_{2m}(\hat{\boldsymbol{r}})|^2\, g(r). \quad (10)$$

TABLE VI. Magnetic dipole term for Co monolayers and adatoms on Pd(100), Pd(111), and Pd(110) (optimized geometries) for different magnetization directions. For each system, the first line ("exact") contains values calculated using Eq. (5) and the second line ("approx.") contains values calculated using Eq. (9). The T_y terms were evaluated only for the (110) surface.

		T_z	T_x	T_y	$7(T_x - T_z)$	$7(T_y - T_z)$
			Co on Pd(100)			
Monolayer	Exact	−0.017	0.010		0.188	
	Approx.	−0.018	0.009		0.184	
Adatom	Exact	−0.024	0.015		0.275	
	Approx.	−0.026	0.013		0.276	
			Co on Pd(111)			
Monolayer	Exact	−0.066	0.035		0.707	
	Approx.	−0.069	0.034		0.723	
Adatom	Exact	−0.146	0.080		1.577	
	Approx.	−0.154	0.077		1.618	
			Co on Pd(110)			
Monolayer	Exact	−0.057	−0.008	0.068	0.339	0.872
	Approx.	−0.060	−0.009	0.069	0.360	0.904
Adatom	Exact	−0.112	−0.020	0.141	0.644	1.768
	Approx.	−0.117	0.011	0.106	0.900	1.566

The sum $\sum_j$ goes over neighboring magnetic atoms located at positions $\boldsymbol{R}_j$. Substrate atoms could be included in this sum as well (with an *ad hoc* weighting coefficient) but this has no big influence on the outcome. Concerning the electron density, as a first guess we model it by a normalized Gaussian curve

$$g(\boldsymbol{r}) = \exp\left[-4\ln 2\left(\frac{r}{w}\right)^2\right],$$

with full width at half maximum w equal to the Wigner-Seitz radius. Directional m-dependent coordination numbers obtained in this way for Co atoms in the monolayers are presented in Table VII.

Analogously to previous studies on free[1] and supported clusters,[2,44] we further assume a linear dependence of $\mu_{\text{spin}}^{(m)}$ on c_m:

$$\mu_{\text{spin}}^{(m)} = -ac_m + b. \tag{11}$$

One can think of several ways to determine the a and b coefficients: we adopted here one that is technically simple and does not require much input information. In particular, considering the calculated values of $\mu_{\text{spin}}^{(m)}$ shown in Table V, we set the coefficients a and b in Eq. (11) by requiring that for each investigated system (characterized by a set of c_m coefficients) the lowest $\mu_{\text{spin}}^{(m)}$ should be 0.35 μ_B and the largest $\mu_{\text{spin}}^{(m)}$ should be 0.50 μ_B. After that, we apply an overall normalization so that the total μ_{spin} is always 2.07 μ_B (which is the average value of μ_{spin} for Co monolayers on all three surfaces). The values of $\mu_{\text{spin}}^{(m)}$ obtained thereby are then substituted into formula (9) to get model values for T_α. The results are shown in Table VIII. If the model is changed a bit, e.g., if the width w of the Gaussians in Eq. (10) is varied by 50%–200%, or if the coefficients a, b in Eq. (11) are determined by using information more specific to each of the surfaces, or if the Pd atoms are partially included in defining the c_m coefficients, the results shown in Table VIII do not change significantly.

When comparing the model values in Table VIII with the calculated values in Table V, one sees that the simple framework of directional coordination numbers accounts for some trends in T_α. In particular, the sign of T_α is always reproduced correctly [apart from the very small value of T_x for Co on Pd(110)]. For Co on Pd(111), the model works very well. For Co on Pd(110) and Co on Pd(100), the values are quantitatively not so good but the dependence of the T_α term on the magnetization direction is well described.

TABLE VII. Directional coordination numbers c_m for Co atoms in monolayers on Pd(100), Pd(111), and Pd(110) evaluated according to Eq. (10), in a basis of real spherical harmonics.

m	Pd(100)	Pd(111)	Pd(110)
xy	0.0464	0.0536	0.0104
yz	0.0108	0.0179	0.0104
$3z^2 - r^2$	0.0173	0.0283	0.0095
xz	0.0108	0.0177	0.0015
$x^2 - y^2$	0.0192	0.0536	0.0256

IV. DISCUSSION

We investigated how the magnetic properties of Co adatoms and monolayers can be manipulated by selecting different supporting Pd surfaces. We found that this has a moderate effect on μ_{spin}, larger effect on μ_{orb}, and dramatic effect on

TABLE VIII. Model values of the magnetic dipole term T_α for Co monolayers on Pd(100), Pd(111), and Pd(110) obtained by assuming a linear dependence of $\mu_{\text{spin}}^{(m)}$ on the directional coordination numbers c_m.

Surface	$T_z^{(m)}$	$T_x^{(m)}$	$T_y^{(m)}$
(100)	−0.041	0.020	0.020
(111)	−0.070	0.035	0.035
(110)	−0.035	0.006	0.028

the MAE and on the T_α term. For the adatoms, the effect is larger than for the monolayers. Moreover, the transition from monolayers to adatoms has a larger effect than a moderate variation in the height of the Co layer above the substrate. If the SOC is not very strong, the T_α term can be understood as arising from a competition between those m-decomposed components of $\mu_{\rm spin}$ which are associated with the α coordinate and those which are not.

In the past, the influence of the orientation of superlattices (multilayers) on magnetic properties was already investigated, however, the focus was mainly on the role of defects and interface abruptness.[45] Here, we deal with perfect monolayers and surfaces and investigate how sole selection of a different surface can affect various quantities related to magnetism. Likewise, the importance of the T_z term for an XMCD sum-rule analysis has been highlighted before when it was found that the absolute value of $7T_z$ amounts to about 20% of $\mu_{\rm spin}$ for some low-dimensional systems[12] or that for atomic clusters $\mu_{\rm spin}$ can show a different behavior with changing cluster size when compared to $\mu_{\rm spin} + 7T_z$.[13] In this study, the importance of the *anisotropy* of the magnetic dipole term in nanostructures is stressed and quantitatively assessed for a set of related adatoms and monolayers for the first time.

It should be noted that the anisotropy of T_α which we highlight here is primarily connected with the breaking of the crystal symmetry at the surface and occurs even without SOC. Moreover, we demonstrated that a semiquantitative estimate of this anisotropy can be made by assuming a linear dependence of $\mu_{\rm spin}^{(m)}$ on m-dependent coordination numbers c_m. We also verified that a simplified relation linking T_α to a weighted sum of m-resolved components of $\mu_{\rm spin}$ is satisfied for Co-Pd systems to a great accuracy. We assume that this will be the case for other systems containing $3d$ and $4d$ elements as well. This justifies *a posteriori* the use of this approach to estimate T_α of a Co monolayer by Stöhr and König.[14]

For the monolayers, the changes in $\mu_{\rm spin}$ when going from one surface to another reflect the corresponding changes in the coordination numbers: $\mu_{\rm spin}$ is largest for the (110) monolayer where each Co atom has only two nearest-neighboring Co atoms, next comes the (100) monolayer with four Co neighbors, and the lowest $\mu_{\rm spin}$ is obtained for the (111) monolayer with six Co neighbors. This complements an analogous trend found earlier for free[1] and supported clusters.[2,3,44] The magnetic moments induced at individual Pd atoms are larger for Co monolayers than for Co adatoms, which reflects the fact that for monolayers, Pd atoms are polarized by more than one Co atom.

The sizable intraplanar anisotropy $E^{(x)} - E^{(y)}$ which we get for a Co monolayer on Pd(110) was expected as this system could be viewed as a set of Co wires which are surely anisotropic in this respect. However, we get a very strong azimuthal dependence of the MAE also for the *adatom* on the (110) surface which is not so obvious as this can be only caused by the underlying substrate. The (110) fcc surface has a rectangular symmetry with a clearly present x-y anisotropy. At the same time, however, the magnetic moments at Pd atoms are not very large (Table III), neither is the SOC parameter ξ for Pd in comparison to, e.g., $5d$ elements. So, one might assume that the influence of the substrate x-y asymmetry would not be very strong in this case. Thus, the large $E^{(x)} - E^{(y)}$ anisotropy energy for a Co adatom on Pd(110) can be seen as an example of the high sensitivity of the MAE. We should note that a strong azimuthal dependence of the MAE for adatoms was observed also for the CuN/Cu(001) surface.[46] However, in that case, the magnetic adatom was in a bridge position meaning that the x-y symmetry breaking was more immediate than in the case of an adatom in a hollow position. As a final remark, we would like to mention that the calculated azimuthal dependencies of the MAE can be accurately fitted by smooth sinusoidal curves (see Fig. 5), which indicates a very good numerical stability of the computational procedure.

The intraplanar anisotropy for a Co adatom on the Pd(111) surface can be compared to similar systems investigated in the past. In particular, for a Co adatom on Pt(111), the amplitude of the $E^{(\parallel)}(\phi) - E^{(z)}$ curve is about 2% of the average value,[47] i.e., similar to the current case. For a 2×2 surface supercell coverage of Fe on Pt(111), this amplitude is 10%–25% (depending on the geometry relaxation);[48] this relatively large value with respect to our case is very probably due to the fact that the 2×2 surface supercell is already quite distinct from the isolated adatom we discuss here.

In the past, a lot of attention was paid to Co/Pd *multilayers*, especially in connection with the MAE. In some respects, multilayers and monolayers behave in a similar way. For example, concerning how much the out-of-plane magnetization is preferred by the Pd(111)-related system in comparison with the Pd(100)-related systems. In particular, according to our calculations, a Co monolayer on Pd(100) has an in-plane magnetic easy axis, a Co monolayer on Pd(111) has an out-of-plane magnetic easy axis, and the difference between the respective MAE values is about 1 meV. According to an earlier work on Co/Pd multilayers,[49] both Co_1Pd_3 (100) and Co_1Pd_2 (111) multilayers have an out-of-plane magnetic easy axis, but the MAE per unit cell is by about 0.9 meV larger for the (111) multilayer than for the (100) multilayer.

Likewise, the dependence of the MAE on $E_{\rm band}$ seems to have a similar character for the multilayers (or slabs) and for the monolayers: the $E^{(x)} - E^{(z)}$ value is decreasing with increasing $E_{\rm band}$ for the (100) crystallographic orientation (cf. $Pd_2Co_1Pd_2$ slab studied by Wang *et al.*)[50] and relatively unchanging with $E_{\rm band}$ in the vicinity of E_F for the (111) orientation (cf. Co_1Pd_2 multilayer studied by Daalderop *et al.*),[51] which resembles our results shown in Fig. 4. However, as mentioned in the Introduction, one has to be careful when comparing theoretical results obtained by different studies because the MAE is quite sensitive to the technical details of the calculation. One should also bear in mind that the results on Co/Pd multilayers and slabs depend on the number of the interlaying Pd layers (cf. Ref. 52 for the sensitivity of the MAE to the slab thickness).

The theoretical values for the anisotropy of T_α shown in Table VI can be compared with experimental data for a similar system, namely, a single Co(111) layer sandwiched between two thick Au layers. By extrapolating results obtained via angle-dependent XMCD measurements, Weller *et al.*[53] obtained $7T_x = 0.43\ \mu_B$ and $7T_z = -0.86\ \mu_B$. Our values for a Co monolayer on Pd(111), $7T_x = 0.24\ \mu_B$ and $7T_z = -0.46\ \mu_B$ (see Table VI), are fully consistent with this. One should also note that our values for a Co monolayer on Pd(111) are quite similar to earlier results for a Co layer sandwiched between few Pd(111) layers (where $7T_\alpha$ is 0.18 μ_B and

$-0.34\ \mu_B$ for an in-plane and out-of-plane orientation of the magnetization, respectively),[39] which suggests that comparing theoretical data for a monolayer with experimental data for a sandwich is relevant in this case.

We expect that our values for $\mu_{\rm orb}$ will be systematically smaller than experimental values because we rely on the LSDA which usually underestimates $\mu_{\rm orb}$.[54,55] The same may be also true for the MAE. However, this does not affect our conclusions.

We used potentials subject to the ASA which may limit the numerical accuracy of our results, particularly as concerns the MAE. On the other hand, our results do not differ too much from results of full-potential calculations, especially in the case of monolayers. For a Co monolayer on Pd(100), we get an in-plane magnetic easy axis with an MAE of -0.73 meV per Co atom while Wu *et al.*[56] obtained for the same $z_{\text{Co-Pd}}$ distance (1.65 Å) a theoretical MAE of -0.75 meV. Magneto-optic Kerr measurements[17] as well as XMCD experiments[57] showed that the magnetic easy axis of ultrathin Co films on Pd(100) is indeed in plane (the experiment includes also an in-plane contribution from the shape anisotropy). Note that the theoretical MAE of -0.18 meV given in Ref. 17 was obtained for a partially disordered Co monolayer simulating the growth conditions, so it can not be directly compared to our results obtained for an ideal monolayer.

For a Co monolayer on Pd(111), we get a $\mu_{\rm spin}$ value of 2.01 μ_B in a Co ASA sphere with a radius of 1.46 Å while the full-potential calculations of Wu *et al.*[19] led to a $\mu_{\rm spin}$ value of 1.88 μ_B obtained within a Co muffin-tin sphere with a radius of 1.06 Å. Both calculations thus again give consistent results. For Pd atoms just below the Co layer, we get a $\mu_{\rm spin}$ value of 0.32 μ_B in a sphere with a radius of 1.49 Å while the corresponding $\mu_{\rm spin}$ value of Wu *et al.*[19] obtained within a sphere having a radius of 1.32 Å is 0.37 μ_B. In this last case, one has to bear in mind that Wu *et al.*[19] used a thin slab of only five Pd layers sandwiched between two Co layers which clearly favors a larger Pd polarization in comparison with just a single Co-Pd interface considered in this work.

For adatoms, the ASA may be more severe than for monolayers, nevertheless, the agreement between our calculations and the results obtained via a full potential calculation is pretty good (see the end of the Appendix). As a whole, the accuracy of our calculations is sufficient to warrant the conclusions which rely on comparing a large set of data and not only on results for a singular system.

It follows from our results that one can change the magnetic easy axis from in-plane to out-of-plane direction just by using as a substrate another surface of the same element. This could be used as yet another ingredient for engineering the MAE of nanostructures, which has become a great challenge recently.[58] We also showed that the magnetic dipole T_α term can mimic a large anisotropy of $\mu_{\rm spin}$ when determined from the XMCD sum rules. Hence, the anisotropy of T_α has to be taken fully into account when analyzing XMCD experiments on nanostructures.

V. CONCLUSIONS

Co monolayers and adatoms adsorbed on different surfaces of Pd exhibit quite different magnetic properties. Changing the surface orientation has a moderate effect on $\mu_{\rm spin}$ but a large effect on $\mu_{\rm orb}$ (the differences in $\mu_{\rm spin}$ when going from one surface to another are less than 10%, while the differences in $\mu_{\rm orb}$ are 20%–50%). The effect on the MAE may be crucial: selecting a different surface can change the direction of the magnetic easy axis. Similar trends occur when comparing monolayers and adatoms: For $\mu_{\rm spin}$, the differences between monolayers and adatoms are only quantitative, for $\mu_{\rm orb}$ the differences are large, and for MAE the differences are substantial. For the monolayers, the changes in $\mu_{\rm spin}$ when going from one surface to another reflect the corresponding changes in the coordination numbers. A surprisingly strong azimuthal dependence of the MAE is predicted for a Co adatom on Pd(110). For high-symmetry surfaces, on the other hand, varying the azimuthal angle changes the MAE of adatoms by less than a few percent.

The magnetic dipole term T_α which characterizes the anisotropy of the spin density distribution depends substantially on crystallographic orientation of the substrate and also on the direction of the magnetization. As a result of this, a strong apparent anisotropy of $\mu_{\rm spin}$ as deduced from the XMCD sum rules may be falsely observed. For systems with small spin-orbit coupling such as Co/Pd, the T_α term can be accurately described by an approximative formula which relates T_α to the differences between components of the spin magnetic moment resolved according to the magnetic quantum number m. For interpretation of the trends of T_α with the substrate crystallographic orientation, the concept of directional m-dependent coordination number is helpful.

ACKNOWLEDGMENTS

This work was supported by the Grant Agency of the Czech Republic within the Project No. 108/11/0853, by the Bundesministerium für Bildung und Forschung (BMBF) Verbundprojekt Röntgenabsorptionsspektroskopie (Grant No. 05K10WMA), and by the Deutsche Forschungsgemeinschaft (DFG) via SFB 689. Stimulating discussions with P. Gambardella are gratefully acknowledged.

APPENDIX: EFFECT OF THE SIZE OF THE RELAXATION ZONE

When studying the magnetism of adatoms, one should address the question as to which extent the host around the adatom has to be allowed to polarize. Zeller showed[37] that the polarization cloud around a magnetic impurity in bulk Pd extends at least up to 1000 atoms. Šipr *et al.*[52] showed that the convergence of the MAE with respect to the slab thickness and/or with respect to the size of the supercell which simulates the adatom is much slower than the convergence of magnetic moments. In view of these facts, it is desirable to explore more deeply the situation for the systems considered in this work.

As a test case, we select a Co adatom on Pd(111). To facilitate the comparison with calculations done by other methods, we put the Co adatom in an hcp hollow site, with the vertical distance between the Co adatom and the Pd surface layer as $z_{\text{Co-Pd}} = 1.64$ Å. Our system is thus similar to the system investigated by Błoński *et al.*[20] (the main difference with respect to Ref. 20 is that we do not consider any buckling

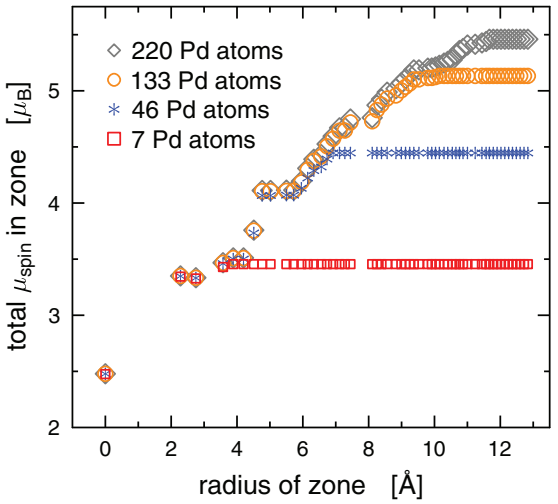

FIG. 6. (Color online) Sum of the spin magnetic moments at the Co adatom and at those substrate Pd atoms which are enclosed in hemispherical zones of the given radii, for four embedded cluster sizes (identified by numbers of Pd atoms contained in them).

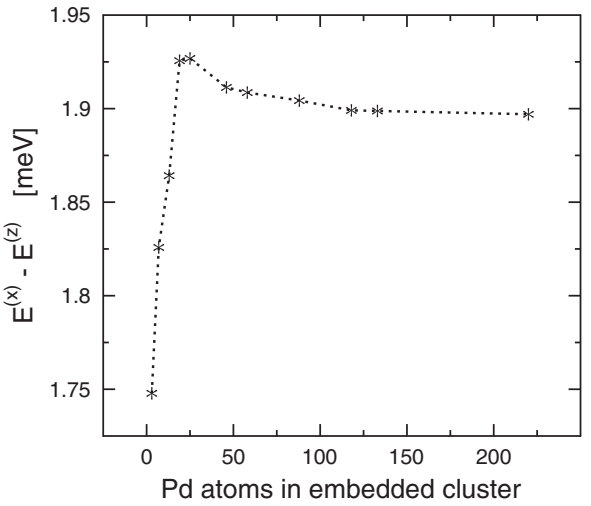

FIG. 7. The MAE of a Co adatom in an hcp position on Pd(111) for different sizes of the embedded clusters.

of the substrate). To check the convergence with respect to the size of the zone where the electronic structure is relaxed, we probed a series of embedded cluster sizes, starting with relaxing the electronic structure just in three Pd atoms (i.e., up to the distance of 2.3 Å from the Co adatom) and ending with relaxing it in 220 Pd atoms (up to 11.7 Å from the Co adatom). To safely accommodate this large embedded cluster, we model the Pd substrate by a slab of 19 layers [contrary to 13 layers used in other calculations involving the Pd(111) surface in this work]. The largest embedded cluster with 220 Pd atoms contains Pd atoms located within the fifth layer below the surface and comprises 329 sites altogether.

First, we investigate the convergence of the spin magnetic moments. This can be achieved by inspecting the total μ_{spin} contained inside a hemisphere stretching from the adatom up to a certain radius. The dependence of this total μ_{spin} on the radius of the hemisphere forms an "integral magnetic profile." This is presented in Fig. 6 for four embedded cluster sizes containing 7, 46, 133, and 220 Pd atoms, respectively. The total μ_{spin} for a sphere with zero radius is obviously just the μ_{spin} value of the Co adatom. With increasing sphere radius, the spin magnetic moments of enclosed Pd atoms are added to it. If the radius of the hemisphere becomes larger than the radius of the embedded cluster, the total μ_{spin} obviously does not change any more because the Pd atoms outside the embedded impurity cluster are nonmagnetic.

It follows from Fig. 6 that the spin magnetic moment of the adatom as well as magnetic moments induced in the nearest Pd atoms are actually already well described by relatively small embedded clusters. However, the total μ_{spin} converges only very slowly with increasing size of the relaxation zone because even quite distant Pd atoms still contribute with their nonzero μ_{spin}. Our results suggest that the magnetic moments on all the Pd atoms do not arise due to a direct interaction with the Co adatom. Rather, the adatom induces a magnetization in its nearest neighbors, then these further induce magnetization in the next coordination shell and so on. The emerging picture of how the magnetism spreads through the Pd host is thus consistent with the picture suggested by Polesya *et al.*[38] in terms of an exchange-enhanced magnetic susceptibility (see Fig. 4 of Ref. 38 and the associated text). A plot analogous to Fig. 6 could also be drawn for μ_{orb} exhibiting the same features as seen in Fig. 6.

Our results on the convergence of the magnetic moments may raise objections about the convergence of the MAE. If embedded clusters containing as much as 220 Pd atoms still do not fully account for the host polarization, can one get reliable results for the MAE, which is sensitive to the way the substrate is treated?[52] To check this, we calculated the MAE for a series of embedded cluster sizes (Fig. 7). One can see that in fact the MAE converges quickly with increasing size of the embedded cluster. Already with a relaxation zone including only 46 Pd atoms, which corresponds to a radius of the hemisphere of 6.9 Å containing Pd from up to the third Pd layer below the surface, the accuracy of the MAE is better than 1%. This means that all the results presented in this work are well converged.

The data in Fig. 7 demonstrate that it is sufficient to include a rather small polarization cloud within the Pd host in order to get convergence in the MAE values. More distant Pd atoms do not contribute to the MAE, *even if they are magnetically polarized*. This conclusion is not in contradiction with an earlier result that reliable values of the MAE can be obtained only if the host is represented by slabs of at least 10 layers[52] because that result concerned the total "physical" size of the model system while in this appendix we focus only on the size of the zone where the electronic structure is allowed to relax to the presence of an adatom (or of an adsorbed monolayer).

To complete this part, we should compare our results with the results of Błoński *et al.*,[20] which were obtained by performing a plane-wave projector-augmented wave (PAW) calculation for a supercell comprising five-layer-thick slabs and a 5×5 surface unit cell. As concerns the Co adatom itself, μ_{spin} and μ_{orb} for the in-plane magnetization direction and μ_{orb} for the out-of-plane magnetization direction are 2.48 μ_B,

0.15 μ_B, and 0.27 μ_B in this work and 2.24 μ_B, 0.19 μ_B, and 0.22 μ_B in Błoński *et al.*[20] As concerns the MAE calculated via the magnetic force theorem (torque method), it is 1.90 meV out of plane in this work and 0.72 meV out of plane in Błoński *et al.*[20] The value for the induced μ_{spin} in the nearest Pd atoms is 0.28 μ_B in this work and 0.33 μ_B in Błoński *et al.*[20] All these values are in good agreement, considering the differences between both approaches.

*sipr@fzu.cz

[1] O. Šipr, M. Košuth, and H. Ebert, Phys. Rev. B **70**, 174423 (2004).

[2] P. Mavropoulos, S. Lounis, R. Zeller, P. H. Dederichs, and S. Blügel, Appl. Phys. A **82**, 103 (2006).

[3] S. Bornemann, O. Šipr, S. Mankovsky, S. Polesya, J. B. Staunton, W. Wurth, H. Ebert, and J. Minár, Phys. Rev. B **86**, 104436 (2012).

[4] P. Gambardella, A. Dallmeyer, K. Maiti, M. C. Malagoli, W. Eberhardt, K. Kern, and C. Carbone, Nature (London) **416**, 301 (2002).

[5] J. T. Lau, A. Föhlisch, R. Nietubyc, M. Reif, and W. Wurth, Phys. Rev. Lett. **89**, 057201 (2002).

[6] P. Gambardella, S. Rusponi, M. Veronese, S. S. Dhesi, C. Grazioli, A. Dallmeyer, I. Cabria, R. Zeller, P. H. Dederichs, K. Kern, C. Carbone, and H. Brune, Science **300**, 1130 (2003).

[7] P. Carra, B. T. Thole, M. Altarelli, and X. Wang, Phys. Rev. Lett. **70**, 694 (1993).

[8] B. T. Thole, P. Carra, F. Sette, and G. van der Laan, Phys. Rev. Lett. **68**, 1943 (1992).

[9] P. Gambardella, S. S. Dhesi, S. Gardonio, C. Grazioli, P. Ohresser, and C. Carbone, Phys. Rev. Lett. **88**, 047202 (2002).

[10] S. Stepanow, A. Mugarza, G. Ceballos, P. Moras, J. C. Cezar, C. Carbone, and P. Gambardella, Phys. Rev. B **82**, 014405 (2010).

[11] R. Q. Wu and A. J. Freeman, Phys. Rev. Lett. **73**, 1994 (1994).

[12] M. Komelj, C. Ederer, J. W. Davenport, and M. Fähnle, Phys. Rev. B **66**, 140407(R) (2002).

[13] O. Šipr, J. Minár, and H. Ebert, Europhys. Lett. **87**, 67007 (2009).

[14] J. Stöhr and H. König, Phys. Rev. Lett. **75**, 3748 (1995).

[15] M. Komelj, C. Ederer, and M. Fähnle, Phys. Rev. B **69**, 132409 (2004).

[16] P. Krüger, M. Taguchi, and S. Meza-Aguilar, Phys. Rev. B **61**, 15277 (2000).

[17] H. L. Meyerheim, M. Przybylski, A. Ernst, Y. Shi, J. Henk, E. Soyka, and J. Kirschner, Phys. Rev. B **76**, 035425 (2007).

[18] J. Miyawaki, D. Matsumura, A. Nojima, T. Yokoyama, and T. Ohta, Surf. Sci. **601**, 95 (2007).

[19] R. Wu, C. Li, and A. J. Freeman, J. Magn. Magn. Mater. **99**, 71 (1991).

[20] P. Błoński, A. Lehnert, S. Dennler, S. Rusponi, M. Etzkorn, G. Moulas, P. Bencok, P. Gambardella, H. Brune, and J. Hafner, Phys. Rev. B **81**, 104426 (2010).

[21] S. H. Vosko, L. Wilk, and M. Nusair, Can. J. Phys. **58**, 1200 (1980).

[22] H. Ebert, D. Ködderitzsch, and J. Minár, Rep. Prog. Phys. **74**, 096501 (2011).

[23] H. Ebert and R. Zeller, SPR-TB-KKR package, http://olymp.cup.uni-muenchen.de.

[24] R. Zeller, P. H. Dederichs, B. Újfalussy, L. Szunyogh, and P. Weinberger, Phys. Rev. B **52**, 8807 (1995).

[25] S. Bornemann, J. Minár, S. Polesya, S. Mankovsky, H. Ebert, and O. Šipr, Phase Transitions **78**, 701 (2005).

[26] R. R. Birss, *Symmetry and Magnetism*, Selected Topics in Solid State Physics, Vol. 3 (North-Holland, Amsterdam, 1966).

[27] X. D. Wang, R. Q. Wu, D. S. Wang, and A. J. Freeman, Phys. Rev. B **54**, 61 (1996).

[28] J. B. Staunton, L. Szunyogh, A. Buruzs, B. L. Gyorffy, S. Ostanin, and L. Udvardi, Phys. Rev. B **74**, 144411 (2006).

[29] S. Bornemann, J. Minár, J. Braun, D. Ködderitzsch, and H. Ebert, Solid State Commun. **152**, 85 (2012).

[30] P. Bruno, Phys. Rev. B **39**, 865 (1989).

[31] H. A. Dürr, G. Y. Guo, G. van der Laan, J. Lee, G. Lauhoff, and J. A. C. Bland, Science **277**, 213 (1997).

[32] P. Ravindran, A. Kjekshus, H. Fjellvåg, P. James, L. Nordström, B. Johansson, and O. Eriksson, Phys. Rev. B **63**, 144409 (2001).

[33] C. Andersson, B. Sanyal, O. Eriksson, L. Nordström, O. Karis, D. Arvanitis, T. Konishi, E. Holub-Krappe, and J. Hunter Dunn, Phys. Rev. Lett. **99**, 177207 (2007).

[34] O. Šipr, J. Minár, S. Mankovsky, and H. Ebert, Phys. Rev. B **78**, 144403 (2008).

[35] R. Skomski, A. Kashyap, and A. Enders, J. Appl. Phys. **109**, 07E143 (2011).

[36] G. van der Laan, J. Phys.: Condens. Matter **10**, 3239 (1998).

[37] R. Zeller, Modelling Simul. Mater. Sci. Eng. **1**, 553 (1993).

[38] S. Polesya, S. Mankovsky, O. Šipr, W. Meindl, C. Strunk, and H. Ebert, Phys. Rev. B **82**, 214409 (2010).

[39] G. Y. Guo and H. Ebert, Phys. Rev. B **53**, 2492 (1996).

[40] J. Stöhr, J. Electron. Spectrosc. Relat. Phenom. **75**, 253 (1995).

[41] J. Stöhr, J. Magn. Magn. Mater. **200**, 470 (1999).

[42] H. A. Dürr and G. van der Laan, Phys. Rev. B **54**, R760 (1996).

[43] C. Ederer, M. Komelj, J. W. Davenport, and M. Fähnle, J. Electron. Spectrosc. Relat. Phenom. **130**, 97 (2003).

[44] O. Šipr, S. Bornemann, J. Minár, S. Polesya, V. Popescu, A. Šimůnek, and H. Ebert, J. Phys.: Condens. Matter **19**, 096203 (2007).

[45] C. H. Lee, R. F. C. Farrow, C. J. Lin, E. E. Marinero, and C. J. Chien, Phys. Rev. B **42**, 11384 (1990).

[46] A. B. Shick, F. Máca, and A. I. Lichtenstein, Phys. Rev. B **79**, 172409 (2009).

[47] S. Bornemann, J. Minár, J. B. Staunton, J. Honolka, A. Enders, K. Kern, and H. Ebert, Eur. Phys. J. D **45**, 529 (2007).

[48] M. Tsujikawa, A. Hosokawa, and T. Oda, J. Phys.: Condens. Matter **19**, 365208 (2007).

[49] K. Kyuno, J. Ha, R. Yamamoto, and S. Asano, J. Phys.: Condens. Matter **8**, 3297 (1996).

[50] D.-S. Wang, R. Wu, and A. J. Freeman, Phys. Rev. B **48**, 15886 (1993).

[51] G. H. O. Daalderop, P. J. Kelly, and M. F. H. Schuurmans, Phys. Rev. B **50**, 9989 (1994).

[52] O. Šipr, S. Bornemann, J. Minár, and H. Ebert, Phys. Rev. B **82**, 174414 (2010).

[53] D. Weller, J. Stöhr, R. Nakajima, A. Carl, M. G. Samant, C. Chappert, R. Mégy, P. Beauvillain, P. Veillet, and G. A. Held, Phys. Rev. Lett. **75**, 3752 (1995).

[54]O. Hjortstam, J. Trygg, J. M. Wills, B. Johansson, and O. Eriksson, Phys. Rev. B **53**, 9204 (1996).
[55]S. Chadov, J. Minár, M. I. Katsnelson, H. Ebert, D. Ködderitzsch, and A. I. Lichtenstein, Europhys. Lett. **82**, 37001 (2008).
[56]R. Wu, L. Chen, and A. J. Freeman, J. Magn. Magn. Mater. **170**, 103 (1997).
[57]M. Sawada, T. Tagashira, K. Furumoto, T. Ueno, A. Kimura, H. Namatame, and M. Taniguchi, J. Electron. Spectrosc. Relat. Phenom. **184**, 280 (2011).
[58]S. Ouazi, S. Vlaic, S. Rusponi, G. Moulas, P. Buluschek, K. Halleux, S. Bornemann, S. Mankovsky, J. Minár, J. B. Staunton, H. Ebert, and H. Brune, Nat. Commun. **3**, 1313 (2012).